

Numerical Modelling and Experimental Investigation of a Buried Arc Welding Process

¹Bestprojekt, Bureau of Energetics and Mechanical Engineering Ltd., Zagreb, Croatia

²Faculty of Mechanical Engineering and Naval Architecture, University of Zagreb, Zagreb, Croatia

Abstract

This paper presents a numerical and experimental study of residual stresses induced by the buried arc welding process in a butt-welded plate sample. Within the framework of numerical investigations, a thermo-mechanical finite element analysis is performed by applying the element birth and death technique in the thermal analysis, while the mechanical analysis is performed simultaneously in one step to reduce simulation time. To validate the numerical model, a series of experiments using a fully automated welding process are conducted. The temperature and residual stress measurements are performed by using thermocouples and hole-drilling stress relaxation method. Furthermore, the heat input efficiency for the buried arc welding process is determined by using a parametric analysis.

Keywords: *buried arc welding, butt-welded plates, residual stress, modified MAG welding, thermocouples, hole-drilling method.*

1. Introduction

Butt joint and T-joint welded plates are frequently used in shipbuilding, offshore, power plants, civil engineering and many other industrial fields as fundamental members of various structures. In engineering practice, the welding of such structures is commonly performed by Metal Active Gas (MAG) welding technique that is accompanied with a large heat input, which leads to local melting of the material through the addition of a molten metal electrode. An inevitable and harmful consequence of this process is that due to the rapid cooling in the material, residual stresses and permanent deformations occur with microstructural changes in the welded joint. In the presence of cracks in the material, tensile residual stresses

in combination with workload accelerate their growth and lead to shorter life of structures [1].

The main disadvantages of such conventional MAG welding procedure are visible in the welding of thick plates where a huge number of weld passes are needed that significantly increases production time [2]. A reasonable solution to the high-productive welding of thick plates could be in a modified MAG welding process that utilizes the specific high penetration arc phenomena i.e. buried arc. This type of arc has been known from earlier but is very rarely used in MAG welding due to its arc instability. In recent years, due to its technical progress, buried arc welding has become a very attractive tool in the welding of thick plates.

Since there is still no adequate data available in the literature for this specific arc mode transfer, the goal of this study is to investigate the thermal and residual stress fields caused by buried arc welding numerically and experimentally. Consequently, it is of great interest to analyse the weld joint characteristics as well as thermal history and distortions due to the relatively high heat input and specific heat distribution in the weld pool area.

During the last decades, finite element (FE) simulations of welding processes have become important tools for prediction of welding residual stresses and distortions. In principle, this simulation consists of two main parts: thermal analysis and mechanical stress analysis [3–7]. In thermal analysis, the temperature field is determined as a function of time for each integration point. This temperature time-history is used as an input into the thermal stress analysis. Herein, the thermal solution can be sequentially or fully coupled with the mechanical solution of the structure. Because the rate of heat generation due to mechanical dissipation energy can be neglected in the heat transfer analysis, a sequentially coupled thermal-stress

analysis is commonly applied for the simulation of a welding process in which a thermal analysis is followed by a stress analysis [8–11].

In this study, the welding experiments are conducted using the fully automated buried arc welding process. Here, the temperature and residual stress measurements are performed by using thermocouples and hole-drilling stress relaxation method and the test results are compared with those obtained from the finite element analyses. The paper is organized as follows. Section 2 contains a description of the buried arc welding procedure. In Section 3, the experimental set-up is provided where the welding conditions, thermal and residual stress measurements are discussed in detail. Next, in Section 4, the numerical model is presented. Section 5 contains comparisons of the experimentally measured and numerically calculated temperature histories and residual stresses induced by the buried arc welding of two steel plates. Finally, some concluding remarks are given in the last section.

2. Description of buried arc welding process

Enhanced welding productivity is one of the main goals to be achieved and it is projected through two aspects; larger metal deposit and deeper penetration. This is possible to obtain through increase of current and consequently voltage in the electric arc. However, beyond spray arc area severe rotation of the arc is present that is very difficult to control. From this aspect, MAG technology offers variety of so-called modified processes which enable metal transfer and improved operational stability in parameter area where conventional processes are unstable or result with some irregularities like spattering or lack of fusion. Such modified processes could be achieved in low and high end of MAG parameter area, that is to say, at low and high currents. While low currents are suitable for thin plates and root welding, high currents are applied in thick plates welding. The buried arc MAG welding is suitable for application in thick plate welding. The definition of the buried arc emphasizes that due to decreases of the arc voltage, the arc is generated and positioned below the melted metal surface and high currents are simultaneously applied in order to achieve better penetration and higher welding deposits (Fig. 1) [12].

In comparison to the conventional arc interaction, the heat input by the buried arc is applied to a deeper portion of the plate, and thus very deep penetration can be obtained.

Furthermore, comparing to a conventional MAG process which is generally carried out using currents below 500 A, the buried arc utilizes higher currents. Development of equipment that utilizes waveform control where arc continuously pressurizes the side portion of the molten metal using an appropriate current-voltage cycle enables the stable application of the buried arc.

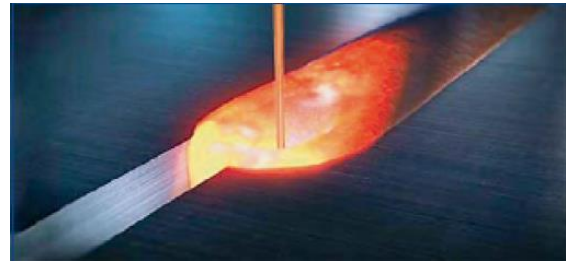


Fig. 1. Buried arc process [13]

From an economical aspect, buried arc application is superior to conventional MAG welding. Due to better penetration, preparation of welding bevels is applied with smaller opening angles. The number of passes can be reduced as well as the complete welding time and the amount of distortions. The consumption of wire and gas is also smaller thus a general cost reduction could be achieved. On the other side, because of high current applications and large deposits, only robotic and automatic means are utilized to perform the process. However, due to high industrial demands the manual process is also being developed. A water-cooled torch is required as well as a robust system for wire feeding as wire speed can achieve up to 60 m/min, depending on the diameter. A detailed comparison between conventional MAG welding and buried arc welding is recently presented in the authors' earlier work [14].

3. Experimental measurements

The geometry of two plates welded into a butt joint, including the relevant dimensions, is presented in Fig. 2. The welding is performed by the buried arc welding procedure using a 7-axis robot system (Fig. 3) supplied by a two parallel 500 A digital inverter power source to ensure sufficient current and to obtain buried arc at high current level. The plates are made of low-carbon steel EN 10025-2: S355J2+N for which the thermal and mechanical properties depending on the temperature and chemical composition are adopted from [14]. A joint preparation with a 3 mm gap and ceramic backing is applied in order to

achieve complete penetration and secure molten metal. A water circulation system has been applied for the closed loop cooling of the torch. The welding parameters chosen for this procedure were as follows: wire diameter 1.6 mm, composition of shielding gas 100% CO₂, gas flow 25 l/min, wire feed speed 12.3 m/min, welding current $I = 540$ A, welding voltage $U = 41$ V and welding speed $v = 300$ mm/min. The welding procedure is completed in a single pass with neutral welding gun inclination.

The temperature measurements during the welding process and cooling time are conducted by two thermocouples (Type K). They are denoted as TC-101 and TC-102 and located in the middle plane of the welded sample, as shown in Fig. 2.

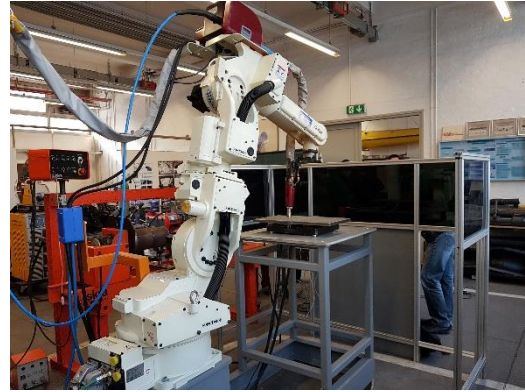


Fig. 3. Experimental setup of two butt-welded plates

For the residual stress measurements, another butt-welded sample is made to eliminate completely the influence of the thermocouple holes on the residual stress state. The measurement of residual stresses is performed by applying the hole-drilling strain-gauge method of stress relaxation using the Vishay RS200 device (Figure 4). The measurement locations of four strain gauges for determination of residual stress are shown in Figure 2.

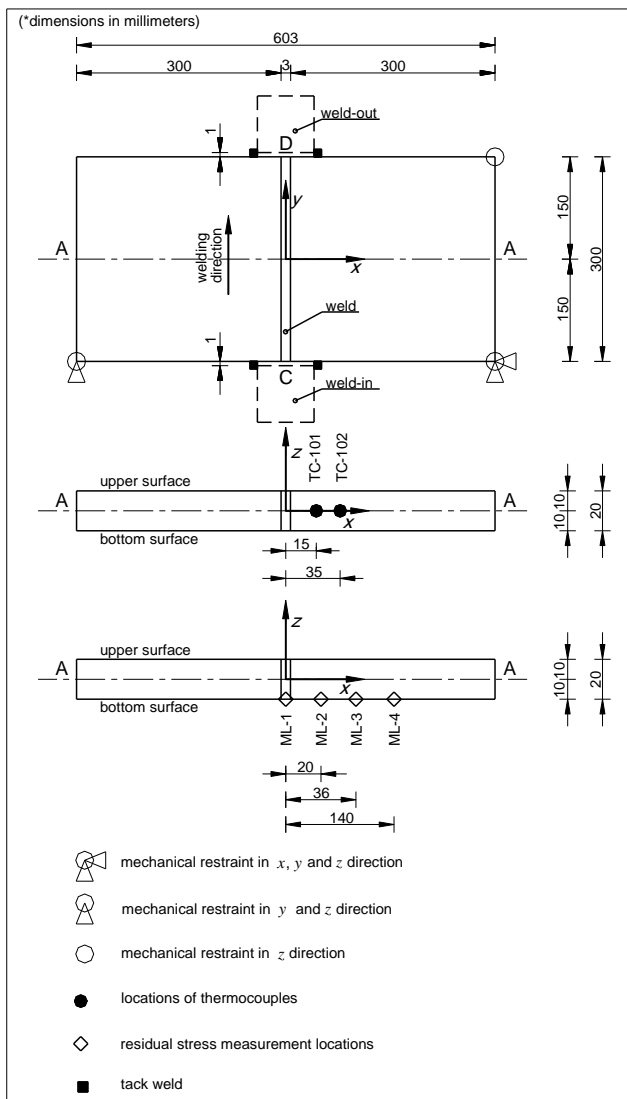


Fig. 2. Geometry of two butt-welded plates



Fig. 4. Measurement of residual stresses

4. Numerical model

As mentioned in the Introduction section, the welding simulation process consists of two independent analyses, i.e. thermal and mechanical ones. In the thermal analysis, the welding process is performed by applying a uniformly distributed heat flux per weld volume, $Q = \eta UI/V_H$, where η represents the efficiency of the heat input and V_H is the heat source volume. The heat flux input applied to the weld is $Q = 6.27 \times 10^{10} \text{ Jm}^{-3}\text{s}^{-1}$. Furthermore, the following data are assumed: the convection heat transfer coefficient $h_c = 10 \text{ Wm}^{-2}\text{K}^{-1}$ and the surface emissivity $\epsilon = 0.9$. In the here presented study, the heat input efficiency for the buried arc welding process is determined using parametric analysis and by varying parameter η until a good match between

the numerically predicted temperatures and experimental measurements has been achieved [15]. It is concluded that the best results are obtained when $\eta = 85\%$, thus this value is taken in the numerical calculations. A similar investigation of welding process efficiency based on the comparison of numerically and experimentally obtained data is performed by Kollár et al [16].

During the thermal analysis, the element birth and death method is applied to simulate weld filler deposition. The obtained temperature-dependent thermal field is then used as an input load in the mechanical analysis. To accelerate the simulation process, a simultaneous weld deposition [17-19] is applied in the mechanical analysis. In the thermal analysis, DC3D8 three-dimensional eight-node brick finite elements are used, while C3D8I elements with incompatible modes are used in the mechanical analysis. Here, an elastic-perfectly plastic behaviour material model is assumed. The mechanical boundary conditions are given in Fig. 2.

The same finite element mesh that consists of 36,960 finite elements (Fig. 5) is used in both thermal and mechanical analysis. A very fine mesh of finite elements is used in the weld bead and its vicinity, while the area far away from the weld is discretised with a coarser mesh to reduce the overall model size. The mesh sensitivity analysis is presented in authors' previous study [14]. In the FE model, it is assumed that the base metal and weld metal have the same thermal and mechanical properties and the creep strains are not taken into account. Moreover, the influence of the phase transformations on the residual stress and deformation state is neglected, as it is insignificant in low-carbon steel [5]. All the computations have been performed within the FE software Abaqus/Standard [20].

5. Results and discussion

5.1. Thermal analysis

The numerically and experimentally obtained temperature-time histories for the first 700 s after the start of welding at the two thermocouple locations TC-101 and TC-102 are given in Fig. 6. As the numerically calculated temperatures are almost identical to the experimentally measured ones, it can be concluded that the implemented thermal material properties are very close to the real ones. The full field

cooling processes for 173 and 381 s after the start of welding are provided in Figs. 7a and 7b.

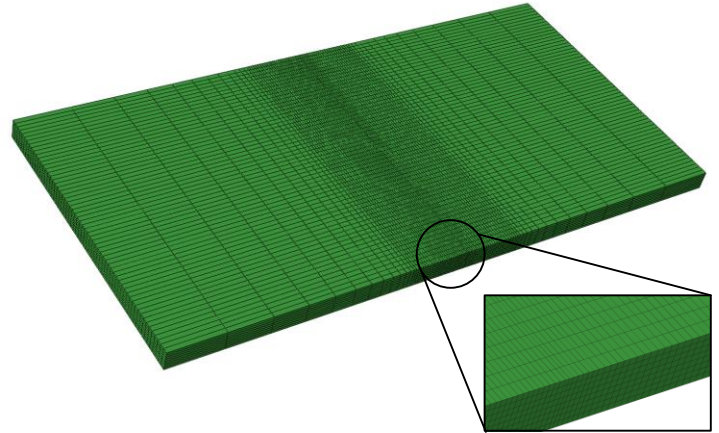


Fig. 5. Finite element mesh of two butt-welded plates

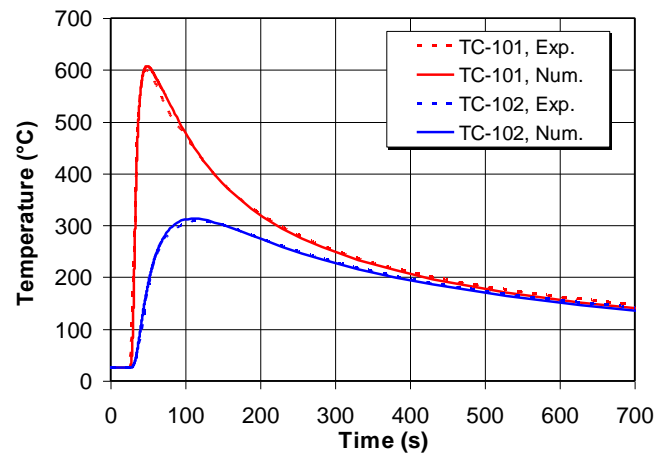


Fig. 6. Temperature-time histories at nodes TC-101 and TC-102

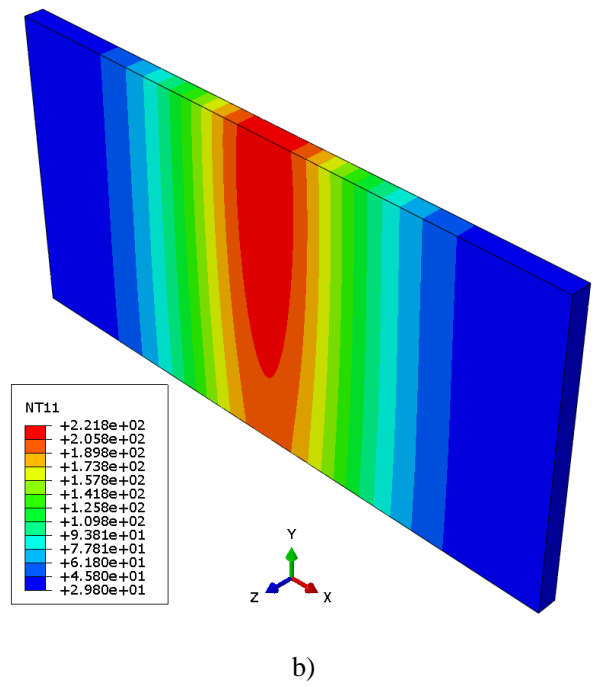
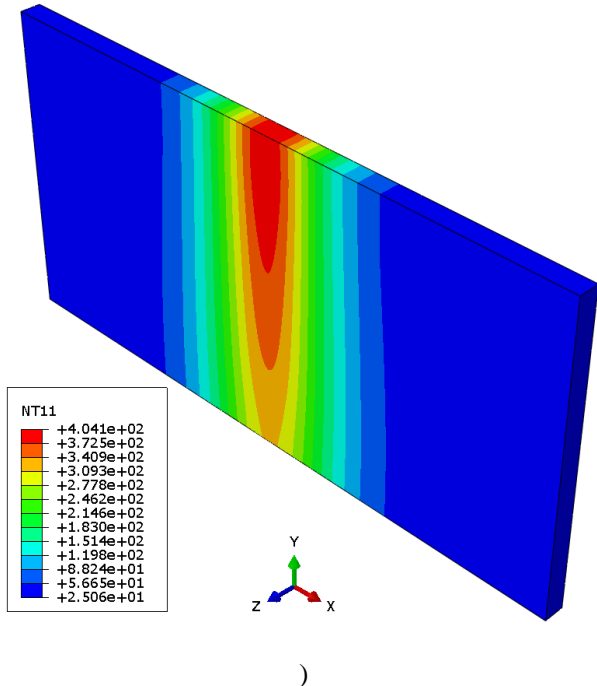


Fig. 7. Full field temperature distributions: a) 173 s after welding start, b) 381 s after welding start

5.2. Mechanical analysis

The residual stresses in the weld direction along the line A-A, seen in Fig. 2, on the lower surface of the plate are presented in Fig. 8. By comparing the numerical and experimental results, it is apparent that their trend is very similar. As seen from Fig. 8, the tensile stresses at the weld line reach the yield strength of the material, which then

decreases to zero, finally becoming compressive at distances far from the weld line. The calculated tensile transversal stress peaks near the weld are 237 MPa (Fig. 9) and vanish at the end of the plates. From Fig. 9, it can be seen that the measured transversal stress approximately follows the numerically calculated one. The difference between the measured and calculated residual stresses can be attributed to the introduced initial stresses during steel production. A feasible procedure to eliminate initial stresses is to anneal the plates at high temperatures. Unfortunately, the annealing procedure before the start of welding is not performed in this study.

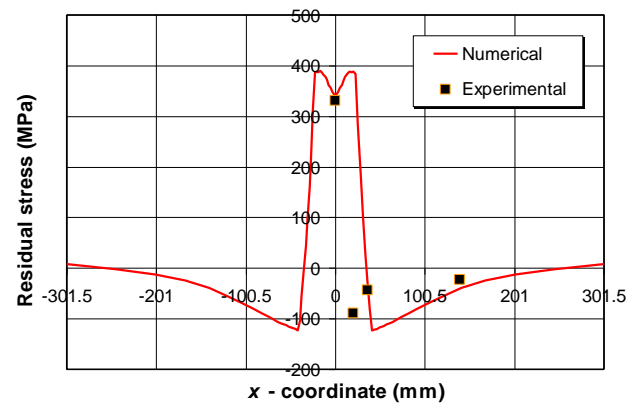


Fig. 8. Residual stresses in the weld direction along the line A-A shown in Fig. 2, on the lower surface of the plate in comparison with experimental measurements

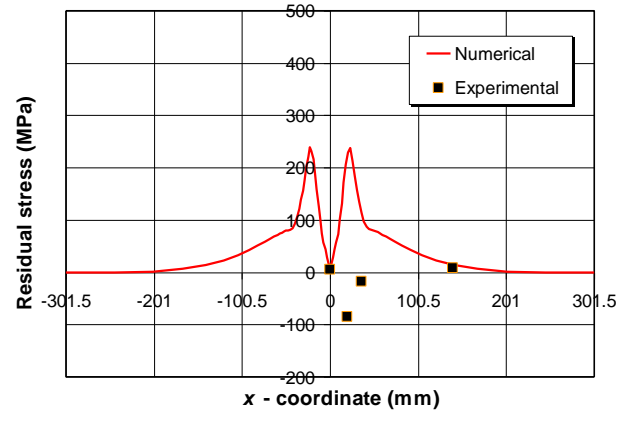


Fig. 9. Transversal residual stresses along the line A-A shown in Fig. 2, on the lower surface of the plate in comparison with experimental measurements

The full field longitudinal and transversal residual stress distributions are given in Fig.s 10a and 10b.

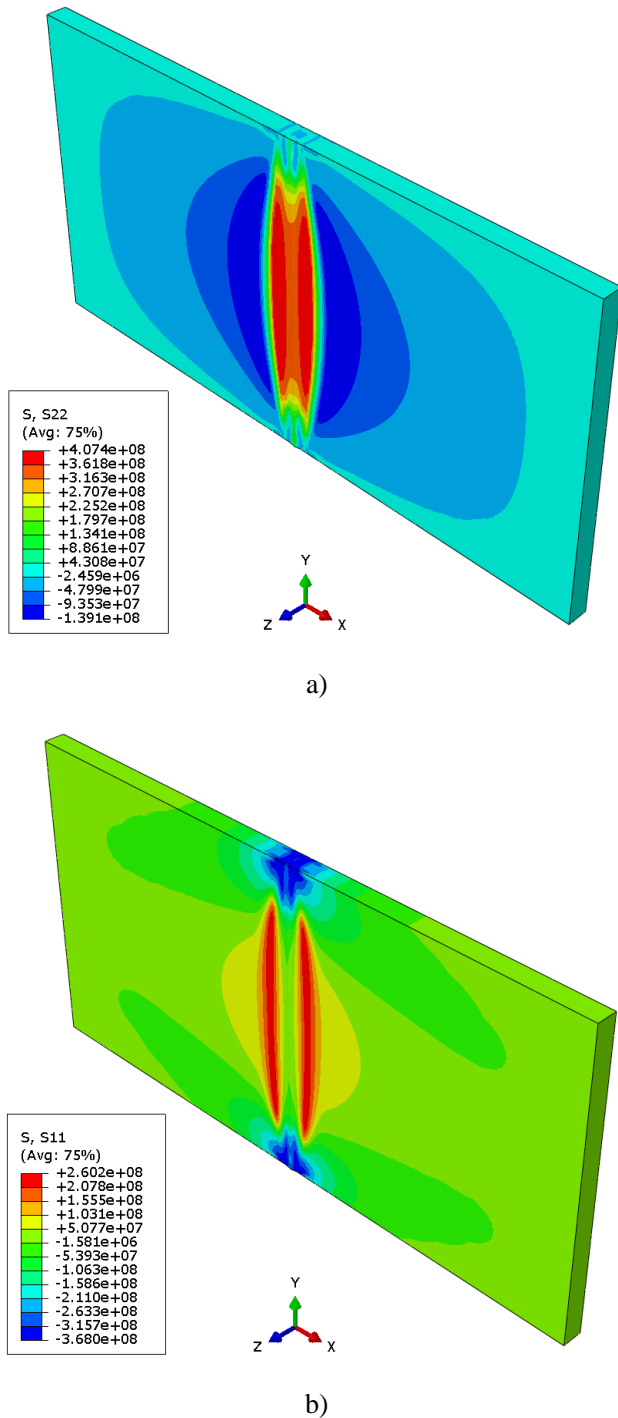


Fig. 10. Full field residual stress distributions: a) longitudinal and b) transversal directions, (N/m^2)

6. Conclusions

In the frame of this study, a numerical model for the simulation of thick steel plate butt-welding using high-productive buried arc technology is proposed and

experimentally validated. In the thermal part of the numerical analysis, the element birth and death method is used for the numerical simulation of filler metal deposition, while a simplified heat flux with uniformly distributed heat flux per weld volume is employed.

The mechanical part of the numerical analysis is done simultaneously in one step to speed up the calculation process. The main conclusions can be summarized as follows:

- The numerically calculated and experimentally measured temperature histories agree very well. The estimated differences are under 1.5%.
- The heat input efficiency for the buried arc welding process is determined using parametric analysis and its value is found to be around 85%.
- The numerically calculated and experimentally obtained longitudinal stresses are tensile in the weld and its vicinity.
- The numerically calculated transversal stresses tend to be about zero in the weld and its vicinity, otherwise they are tensile.

Based on the experimental measurements regarding temperature and residual stress fields, it can be pointed out that the suggested numerical model is suitable for the numerical simulation of buried arc welding.

References

- [1] Chen, Z., Xiong, Y., Qiu, H., Lin, G., Li, Z., Stress intensity factor-based prediction of solidification crack growth during welding of high strength steel. *J Mater Process Technol*, 252, 270–278 (2018).
- [2] Pu, X., Zhang, C., Li, S., Deng, D., Simulating welding residual stress and deformation in a multi-pass butt-welded joint considering balance between computing time and prediction accuracy. *Int J Adv Manuf Technol*, 93(5-8), 2215–2226 (2017).
- [3] Deng, D., Liang, W., Murakawa, H., Determination of welding deformation in filletwelded joint by means of numerical simulation and comparison with experimental measurements. *J Mater Process Technol*, 183, 219–225 (2007).
- [4] Lee, C.H., Chang, K.H., Three-dimensional finite element simulation of residual stresses in

- circumferential welds of steel pipe diameter effects. *Mater Sci Eng A*, 487, 210–218 (2008).
- [5] Deng, D., FEM prediction of welding residual stress and distortion in carbon steel considering phase transformation effects. *Mater Des*, 30, 359–366 (2009).
- [6] Gannon, L., Liu, Y., Pegg, N., Smith, M., Effect of welding sequence on residual stress and distortion in flat-bar stiffened plates. *Mar Struct*, 23, 385–404 (2010).
- [7] Long, H., Gery, D., Carlier, A., Maropoulos P.G., Prediction of welding distortion in butt joint of thin plates. *Mater Des*, 30, 4126–35 (2009).
- [8] Barsoum, Z., Lundback, A., Simplified FE welding simulation of fillet welds – 3D effects on formation residual stresses. *Eng Fail Anal*, 16, 2281–2289 (2009).
- [9] Teng, T.L., Fung, C.P., Chang, P.H., Yang, W.C., Analysis of residual stresses and distortions in T-Joint fillet welds. *Int J Press Vess Pip*, 78, 523–538 (2001).
- [10] Shan, X., Davies, C.M., Wangsdan, T., O'Dowd, N.P., Nikbin, K.M., Thermo-mechanical modelling of a single-bead-on-plate weld using finite element method. *Int J Press Vess Pip*, 86, 110–21 (2009).
- [11] Wang, R., Zhang, J., Serizawa, H., Murakawa, H., Study of welding inherent deformations in thin plates on finite element analysis using interactive substructure method. *Mater Des*, 30, 3474–3481 (2009).
- [12] Baba, H., Era, T., Ueyama, T., Tanaka, M., Single pass full penetration joining for heavy plate steel using high current GMA process. *Weld World*, 61(5), 963-969 (2017).
- [13] Baba, H., Era, T., Ueyama, T., Tanaka, M., Development of high efficiency welding for thick plate steel using stabilized high current buried arc. *Welding* (ISSN 0043-2288), 60(5-6), 121-127 (2017) (in Croatian).
- [14] Perić, M., Garašić, I., Tonković, Z., Vuherer, T., Nižetić, S., Dedić-Jandrek, H., Numerical Prediction and Experimental Validation of Temperature and Residual Stress Distributions in Buried Arc Welded Thick Plates. *Int J Energy Res*, (2019) (in press).
- [15] Jeong, H., Park, K., Cho, J., Numerical analysis of variable polarity arc weld pool. *J Mech Sci Technol*, 30(9), 4307–4313 (2016).
- [16] Kollár, D., Kövesdi, B., Vigh, L.G., Horváth, S., Weld process model for simulating metal active gas welding. *Int J Manuf Technol*, (2019) (in press).
- [17] Perić, M., Tonković, Z., Garašić, I., Vuherer, T., An engineering approach for a T-joint fillet welding simulation using simplified material properties. *Ocean Eng*, 128, 13-21 (2016).
- [18] Perić, M., Tonković, Z., Rodić, A., Surjak, M., Garašić, I., Boras, I., Švaić, S., Numerical analysis and experimental investigation of welding residual stresses and distortions in a T-joint fillet weld. *Mater Des*, 53, 1052-1063 (2014).
- [19] Seleš, K., Perić, M., Tonković, Z., Numerical simulation of a welding process using a prescribed temperature approach. *J Const Steel Res*, 145, 49-57 (2018).
- [20] Abaqus 6.14-1, Dassault Systemes Simulia Corp., Providence, RI, USA, 2014.